Journal of Arid Environments 74 (2010) 540–548

Contents lists available at ScienceDirect

Journal of Arid Environments

journal homepage: www.elsevier.com/locate/jaridenv

Spatio-temporal variations in surface characteristics over the North American Monsoon region

Carlos Lizárraga-Celaya [a,*], Christopher J. Watts [a], Julio C. Rodríguez [b], Jaime Garatuza-Payán [d], Russell L. Scott [e], Juan Sáiz-Hernández [c]

[a] Departmento de Física, Universidad de Sonora, Blvd. Encinas y Rosales, Col. Centro, Hermosillo, Sonora 83000, Mexico
[b] Departmento de Agricultura y Ganadería, Universidad de Sonora, Blvd. Encinas y Rosales, Col. Centro, Hermosillo, Sonora 83000, Mexico
[c] Departmento de Ingeniería Civil y Minas, Universidad de Sonora, Blvd. Encinas y Rosales, Col. Centro, Hermosillo, Sonora 83000, Mexico
[d] Ciencias del Agua y del Medio Ambiente, Instituto Tecnológico de Sonora, Cd. Obregón, Sonora 85000, Mexico
[e] Southwest Watershed Research Center, USDA/Agricultural Research Service, Tucson, Arizona, USA

ARTICLE INFO

Article history:
Received 1 March 2009
Received in revised form
17 September 2009
Accepted 22 September 2009
Available online 18 November 2009

Keywords:
Albedo
Enhanced Vegetation Index
Land surface temperature
MODIS
NAM
North American Monsoon
Variability

ABSTRACT

In this paper we summarize the surface characteristics for six locations in western Mexico and southwestern USA (from a subhumid climate in Jalisco, Mexico to the Sonoran Desert climate in Arizona, USA), that lie along a meridional transect within the North American Monsoon (NAM) core region using available MODerate Resolution Imaging Radiometer (MODIS) satellite data and supplementary surface instrumental data for two of these sites in Sonora, Mexico. The climate analysis for each site is carried out for the period 2000–2008, that includes all available MODIS data. A comparison of seasonal and annual variability in surface conditions for the enhanced vegetation index (EVI), albedo and land surface temperature (LST) at each site is presented. With the help of available surface data from field observations, a more detailed analysis of Rayón and Rosario de Tesopaco sites is presented. The qualitative behavior and climate response of three types of vegetation: desert shrub, subtropical shrub, and tropical deciduous forest ecosystems are analyzed under the influence of the NAM summer wet season. The onset of the NAM warm wet season in early summer, is one of the main precursors of generalized EVI growth in all the NAM region. At all the sites, it is observed that the mean daytime LST cools several degrees as the NAM fully develops. During the warm wet season, in the case of open and sparse vegetation regions such as desert shrub and subtropical shrub, albedo values fall slightly during the NAM season, while in closed and dense tropical deciduous forest regions albedo shows a slight increase. Differences in soil reflectivity at these sites are probably responsible for this rather unexpected behavior. Additionally it is found that, desert shrub and subtropical shrub regions in northern latitudes show large LST and small EVI/albedo seasonal variability, whilst tropical deciduous forests in lower latitudes show much larger EVI/albedo and smaller LST seasonal variability. Thus MODIS data proves to be a valuable tool for assessing the dynamics of seasonal and interannual surface characteristics helpful in determining climate patterns.

1. Introduction

There have been a significant number of contributions in the last two decades addressing the characterization of the North American Monsoon System (NAM), Douglas et al. (1993); Gochis and Brito Castillo (2006); Higgins et al., (1997); Higgins and Gochis (2007). The main focus of these studies is the characterization of the spatio-temporal patterns of warm season precipitation across the NAM region. At the present time there is a better understanding of the diurnal cycle and regional variability of clouds and rainfall as they are related to the complex terrain and continental-maritime regimes.

The characteristic NAM atmospheric pattern was described in detail by Douglas et al. (1993), and can be summarized as one where the precipitation starts shortly afternoon, and most frequently over high elevations on the western slope of the Sierra Madre Occidental (SMO) with modest intensity. Later in the afternoon and evening, at lower elevations, precipitation events occur with less frequency but often with greater intensity. With lower frequency, nocturnal and early morning precipitation occur, generated by shallow clouds over the coasts of the Gulf of California. The NAM system starts early in June at lower latitudes

* Corresponding author. Tel.: + 52 662 259 2242; fax: +52 662 259 2109.
E-mail address: clizarraga@gmail.com (C. Lizárraga-Celaya).

0140-1963/$ – see front matter © 2009 Elsevier Ltd. All rights reserved.
doi:10.1016/j.jaridenv.2009.09.027

(~20°N) in southern Mexico and slowly moves northward along the western slopes of the SMO until it reaches northern latitudes (~35°N) in Arizona and New Mexico by early July, Salinas-Zavala et al. (2001); Watts et al. (2007). For northwestern Mexico the greatest rainfall occurs in July and August (CPC-NWS, 2008).

In this work, we will consider six sites with different latitudes (19.7°N–31.7°N) located in the NAM region (Fig. 1). One site is located in southern Arizona, Lucky Hills, near Tombstone, AZ. Two sites were selected in Sonora, one close to Rayón and one in the surroundings of Rosario de Tesopaco. One more site is in the vicinity of La Paz, in the southern part of the Baja California peninsula on the coast of the Gulf of California. Micrometeorological towers are installed at all these sites and data for evapotranspiration, net radiation, etc., are available for at least four years. Three of the sites (Lucky Hills, Rayón and Rosario de Tesopaco), were included in a detailed study of changes in vegetation condition and surface fluxes during the NAM experiments in 2004 (Watts et al., 2007). The aim of the present work is to extend that analysis to include a) the entire period of MODIS data from 2000–2008 and b) include sites further south in tropical vegetation. The Chamela Biological Reserve in Jalisco is operated by UNAM in Mexico City and has been the subject of numerous ecological and hydrological studies in the last 30 years (e.g. García-Oliva et al. 1995; Maass et al., 1995). It has been designated as a Long Term Ecological Reserve and we intend to initiate surface flux measurements there in 2010. Finally, the site in Tamazula de Victoria Durango was identified as a candidate for future surface flux measurements in the large area between Rosario de Tesopaco and Chamela.

The MODIS products land surface temperature (LST), albedo and enhanced vegetation index (EVI) will be used to study the seasonal and annual evolution of surface characteristics. LST is a physical variable than can give information of the energy balance occurring in land-atmosphere surface processes. The albedo is an indicator of the amount of radiation scattered and dispersed back into the atmosphere and space. And finally, EVI has been designed to improve on Normalized Difference Vegetation Index (NDVI), as a variable for following the greenness of vegetation covers, since it has corrections for some distortions in the reflected light caused by aerosols and ground cover below vegetation, and does not saturate when viewing rain forests and other areas of Earth with large amounts of chlorophyll.

A comparison study of land surface temperature (LST), the enhanced vegetation index (EVI) and albedo will be presented from data for 2000–2008 for all six sites using the MODerate Resolution Imaging Radiometer (MODIS) products available on line. Additionally, with available field data for Rayón and Rosario de Tesopaco, a more detailed description can be made of surface characteristics and albedo comparisons between MODIS composite products and field observations

2. Materials and methods

This study uses MODIS products that are available from 2000 to the present. These data are distributed by the Land Processes Archive Center (LP DAAC), located at the U.S. Geological Survey (USGS) Earth Resources Observation and Science (EROS) Center and can be downloaded from Oak Ridge National Laboratory (daac.ornl.gov). The following three MODIS Land products subsets were used:

1. Land Surface Temperature (LST), (Terra version 5, product MOD11A2)
2. Normalized Difference Vegetation Index (NDVI), Enhanced Vegetation Index (EVI), (Terra version 5, product MOD13Q1)
3. Calculated Albedo (Terra/Aqua version 5 combined, product MCD43A)

The Land Surface Temperature and Emissivity 8-day data products, are composed from the daily 1-km LST product

Fig. 1. Map of sites lying in the NAM core region. Each site is displayed using an asterisk (*) and site labels described in Table 1.

MOD11A1, and stored on a 1-km sinusoidal grid as the average values of clear sky LST during an 8-day period (Wan, 1999). The LST products include the daytime and nighttime temperatures in degrees Kelvin, with supplementary information about the average local time and average view zenith angle of each 1km resolution average temperature data. In this study, only the daytime land surface temperature average registered around 11:00 AM solar time is considered.

The global MODIS vegetation indexes are designed to provide consistent spatial and temporal comparison of vegetation conditions. The blue, red and near infrared reflectance, centered at 469 nm, 645 nm and 858 nm respectively, are combined to determine the MODIS daily vegetation indexes (Huete et al., 1999). The MODIS Normalized Difference Vegetation Index (NDVI) product MOD13Q1, includes a new Enhanced Vegetation Index (EVI) as well, that minimizes canopy background variations, maintaining sensitivity over dense vegetation conditions. The global MOD13Q1 are provided every 16 days at 250 m spatial resolution in a sinusoidal grid projection, and includes not only NDVI and EVI data, but also blue, red and near infrared reflectance, view zenith angle, sun zenith angle, relative azimuth angle. The vegetation indexes are used for monitoring vegetation conditions (Zhang et al., 2003).

While the NDVI index poses some saturation problems over densely vegetated areas, so that the values no longer respond to variations in green biomass, the enhanced vegetation index (EVI) was developed to optimize the vegetation signal with improved sensitivity in high biomass regions and improved vegetation monitoring through a decoupling of the canopy background signal and a reduction in atmospheric influences. This enhanced, soil and atmosphere resistant vegetation index (EVI) has the following expression:

$$\mathrm{EVI} = G(\rho_{\mathrm{nir}} - \rho_{\mathrm{red}})/(L + \rho_{\mathrm{nir}} + C_1\rho_{\mathrm{red}} + C_2\rho_{\mathrm{blue}})$$

where ρ are atmospherically corrected or partially atmosphere corrected (Rayleigh and ozone absorption) surface reflectance, L is the canopy background adjustment that addresses nonlinear, differential near infrared (NIR) and red radiant transfer through a canopy, and C_1, C_2 are the coefficients of the aerosol resistance term, which uses the blue band to correct for aerosol influences in the red band. The coefficients adopted in the EVI algorithm are, $L = 1$, $C_1 = 6$, $C_2 = 7.5$, and the gain factor $G = 2.5$ (Huete et al., 2002).

For the albedo, the MODIS Bidirectional Reflectance Distribution Function (BRDF)/Albedo Model Parameters combined product MCD43A was used, which contains three-dimensional data sets of weighting parameters for the models used to derive the Albedo and other BRDF products. The model supports the spatial relationship and parameter characterization that describe the differences in radiation due to scattering of each pixel, relying on multi-date, atmospherically corrected, cloud-cleared input data measured over 16-day periods at 500 m resolution in a sinusoidal grid projection.

Albedo is defined as the fraction of incident solar radiation that is reflected by a surface. While reflectance is defined as the same fraction for a single incidence angle, albedo is the directional integration of reflectance over all sun-view geometries. Albedo is therefore dependent on the Bidirectional Reflectance Distribution Function (BRDF).

Due to its three-dimensional structure, the Earth's surface scatters radiation anisotropically, especially at the shorter wavelengths that characterize solar irradiance. The Bidirectional Reflectance Distribution Function (BRDF) specifies the behavior of surface scattering as a function of illumination and view angles at a particular wavelength. The albedo of a surface describes the ratio of radiant energy scattered upward and away from the surface in all directions to the down-welling irradiance incident upon the surface. The completely diffuse bihemispherical (or white-sky) albedo can be derived through integration of the BRDF for the entire solar and viewing hemisphere, while the direct beam directional hemispherical (or black-sky) albedo can be calculated through integration of the BRDF for a particular illumination geometry. Actual albedo under particular atmospheric and illumination conditions can be estimated as a function of the diffuse skylight and a proportion between the black-sky and white-sky albedo (Strahler et al., 1999a).

The MODIS/Terra Albedo products provide both the white-sky and the black-sky albedo (at local solar noon) for MODIS bands 1–7 as well as for three broad bands (0.3–0.7 μm, 0.7–5.0 μm, and 0.3–0.5 μm). While the total energy reflected by the earth's surface in the shortwave domain is characterized by the shortwave band 10 (0.3–5.0 μm) broadband albedo, the visible band 08 (0.3–0.5 μm) and near infrared band 09 (0.7–5.0 μm) are also of interest due to marked difference of the reflectance of vegetation in these two spectral regions. Solar radiation is received at the Earth in the shortwave wavelength of 0.3–5.0 μm, with 98% in the range of ~0.3–2.5 μm (Iqbal, 1984).

The MODIS albedo product MCD43A data are based on the Terra and Aqua combined MODIS BRDF/Albedo Model Parameter product MCD43A1. The primary BRDF model parameters from MCD43A1 are used in the equations to calculate black-sky, white-sky and actual (blue-sky) albedo. The calculated data files assumed a solar zenith angle equal to local solar noon and null optical depth. The blue-sky albedo is calculated from a polynomial expression in solar zenith angles, with parameters being provided by the BRDF function for visible, near infrared and shortwave broad bands. The white-sky albedo is calculated from a combination of parameters provided also from the BRDF model for the three previous mentioned broad bands. Finally the actual (blue-sky) albedo is a combination of the black-sky and white-sky albedos with variable function coefficients that depend on the optical depth, solar zenith angle, aerosol type and band (Schaaf et al., 2002).

2.1. Site descriptions

The sites that have been selected are located in the North American Monsoon (NAM) region. They all lie on a transect along the western side of the Sierra Madre Occidental (SMO). There is a collection of works related with NAM influence in some of these sites, Vivoni et al., (2008, in press), Watts et al., (2007). Most of the selected sites have available surface instrumental data and the others are included in future plans for extending the installed micrometeorological network. The sites are the following: one site located in southern Arizona, Lucky Hills (*LH*); two sites in Sonora, Rayón (*RY*) and Rosario de Tesopaco (*RT*); one in Southern Baja California, La Paz (*LP*); Tamazula de Victoria (*TV*) located in the lower sierras of Durango; and one in Jalisco, Chamela (*CH*). The sites are shown in Fig. 1.

According to MODIS Land Type 1, there are 17 classes of land cover in the International Geosphere-Biosphere Programme (IGBP) global classification scheme. In the NAM region studied, the existing land cover classes are: 2) Evergreen Broadleaf Forest, 4) Deciduous Broadleaf Forest, 5) Mixed Forest, 7) Open Shrublands, 8) Woody Savannahs, 9) Savannahs, 10) Grassland, 12) Croplands, 13) Urban and built-up, and 16) Barren or Sparsely vegetated. Classes 1–5 represent forests of different vegetation and densities, while classes 6–12 are related with short and low density vegetation (Strahler et al., 1999b). The site locations and land cover classes are described in detail in Table 1.

In Table 2, the average monthly precipitation (in mm) is presented for climatological stations near the six selected sites. The active NAM months are mostly from June through August, when

Table 1
Summary of sites included in study in Arizona (AZ), Sonora (SON), Baja California Sur (BCS), Durango (DGO) and Jalisco (JAL).

Site	Vegetation type	Location	Lat (°N)	Lon (°W)	Elevation (m)	Shannon DI Richness/Evenness	IGBP land cover classes central/other
LH	Desert Shrub	Lucky Hills Subwatershed, Tombstone, AZ	31.74	110.05	1373.0	2/0.53	10/7
RY	Subtropical Shrub	Rayón, SON	29.74	110.54	616.0	3/0.81	7/8,10
RT	Tropical Deciduous Forest	Rosario de Tesopaco, SON	27.85	109.30	460.0	4/0.85	16/4,5,10
LP	Desert Shrub	La Paz, BCS	24.10	110.31	35.0	3/0.55	7/13,16
TV	Tropical Deciduous Forest	Tamazula de Victoria, DGO	25.0	107.0	526.0	4/0.62	4/2,8,9
CH	Tropical Deciduous Forest	Chamela, JAL	19.65	105.05	183.0	6/0.82	12/4,8,9,10,16

the rainfall each month increases along the north-south gradient for the *TV*, *RT*, *RY* and *LH* sites, with the maximum rainfall occurring in July and August. The maximum monthly precipitation at *CH* and *LP* occurs in September and is presumably due mainly to increased tropical storm activity along the Pacific coast. The *LP* site receives much less rain than the other sites and is not significantly influenced by the NAM system.

The rainfall measurements in the region are not well distributed spatially and only provide daily values. A denser network of more than one hundred tipping bucket rain gauges (TE525, Texas Electronics, Dallas, TX) was installed for the NAM experiment and provided improved information about the spatial and temporal distribution of rainfall as a function of elevation and latitude (Gochis et al., 2003, 2004, 2007). Short-lived, high intensity rainfall is more common at low elevations while longer periods of lower intensity rainfall are more common at higher elevations. The total rainfall increases sharply with elevation on the western slopes of the SMO.

For the present analysis, a square land cover region with sides of approximately 4.25 km, 4.5 km or 5 km length was selected depending on the resolution of the MODIS product (250 m, 500 m or 1 km), for six sites located in the NAM region. The different land cover types for each selected region are shown in Table 1. The heterogeneity of a landscape can be quantified using Shannon Diversity Index (DI) of Richness and Evenness (EuroComm, 2000). Richness is a measure of of the abundance of land cover classes, and evenness is a measure of the relative area of land cover classes.

All available data for the Land Surface Temperature (LST) products MOD11A2, starting date March 5th., 2000 to December 2nd., 2008, was considered for each of the six sites. The 1km tile resolution MODIS land ASCII data, quality controlled filtered data and statistics were obtained for an areal extent of approximately 5 km by 5 km (25 pixels). A time series of average land surface temperatures for each product date was generated by averaging the 8-day average daytime land surface temperatures over all the 1km tiles within the selected region that had similar land class as that of the central tile. In this case, the percentage of tiles in the selected region with same land cover as the central was: *LH* (12% Grassland), *RY* (56% Open shrublands), *RT* (32% Barren or sparsely vegetated), *LP* (16% Barren or sparsely vegetated), *TV* (72% Deciduous broadleaf forest), *CH* (44% Croplands). The Enhanced Vegetation Index (EVI) time series using the available data for MODIS product MOD13Q1, from March 5th, 2000, until December 2nd, 2008. The 250 m tile resolution MODIS land ASCII data and quality controlled filtered data and statistics for each day were obtained for an areal extent of approximately 4.25km wide by 4.25km high (289 pixels). The time series of EVI average values was generated by averaging the 16-day MOD13Q1 EVI over all 250 m tiles within the selected region that had similar land class to that of the central tile. In the EVI case, the following percentage of tiles in the selected region with same land cover as the central one was considered: *LH* (17%), *RY* (51%), *RT* (36%), *LP* (18%), *TV* (70%), *CH* (57%).

The actual shortwave albedo time series where produced using the MODIS MCD43A product, using data from February 26th, 2000 until the processing date December 2nd., 2008. Again the 500 m tile resolution MODIS land ASCII data and quality controlled filtered data and statistics for each available date was obtained for an area extent of approximately 4.5km wide by 4.5km high (81 pixels). The time series of actual shortwave albedo average values was generated averaging the 16-day average shortwave broadband albedos over all 500 m tiles that had similar land class to that of the central tile. For the albedo case, the percentage of tiles in each region having the same land cover as the central one is: *LH* (9%), *RY* (37%), *RT* (14%), *LP* (9%), *TV* (54%), *CH* (16%).

Then the average seasonal variability at each site was obtained by taking the average over all the years for each time period. These are the data plotted for EVI in Fig. 2 and albedo in Fig. 4.

2.2. Surface energy balance measurements

Surface albedo data collected for two sites in Sonora, in a subtropical shrub in Rayón (*RY*) and a tropical deciduous forest in Rosario de Tesopaco (*RT*), are compared with the shortwave actual albedo data from MODIS. The averaged data is presented for the period of June 16th to September 30th, which includes the main Monsoon time period. For the *RY* site, the data collected is for the 2004–2008 period, with the exception of 2005. At the *RT* site, the field measured data covers the complete 2004–2008 period.

In these two sites, surface fluxes of sensible heat and water vapor were measured, using the eddy covariance method. In Rayón (*RY*), a KH Krypton Hygrometer KH20 (CSI – Campbell Scientific Inc., Logan, Utah) was used in 2004 to measure water vapor, and since

Table 2
Precipitation normals (mm) for the selected sites.

Site	Jan	Feb	Mar	Apr	May	Jun	Jul	Aug	Sep	Oct	Nov	Dec	Total
LH	26.16	18.8	18	6.1	6.9	15.8	71.6	78	39.1	32.8	17.5	27.4	358.1
RY	26.7	27.1	10.2	3.1	3.1	16.6	145.9	120.4	51.5	44.9	26.6	38.7	514.8
RT	37.9	17.4	11.7	7	10.1	30.6	208.2	187.8	101.3	36.4	21.3	42.7	712.4
LP	16.7	4	1.6	0.6	1.6	0.6	16	44.1	55.4	11.9	13.3	16.8	182.6
TV	31.1	16.8	5.2	5.8	4.5	68.9	294.9	277.2	169.6	75.5	34	43.4	1026.9
CH	36.9	4.9	1.5	0.5	6.2	88.9	134.1	155.1	219.5	72.2	26.4	10.9	757.1

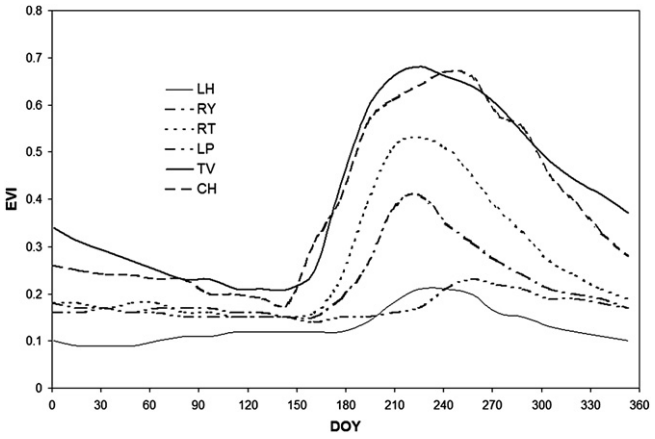

Fig. 2. The average seasonal variability of EVI versus DOY (day of year).

2006 a LI7500 gas analyzer (LI-COR, Lincoln, Nebraska) has provided water vapor and carbon dioxide measurements. In Rosario de Tesopaco (*RT*) a LI7500 gas analyzer has been used to measure water vapor concentrations. At all sites a CNR1 radiometer (Kipp & Zonen, Delft, the Netherlands) was used to measure the four components of radiation: the incoming and outgoing radiation in short and long-wave spectral bands. In addition, CSAT3 (CSI) three-dimensional sonic anemometer were installed at these sites and connected to CR5000 dataloggers (CSI). The data was sampled at a frequency of 10 Hz and the average fluxes were obtained every 30 min.

These sensors are installed several meters above the canopy, in order to be representative of the full exchange of radiation, heat and water flux between the soil + vegetation system and the atmosphere.

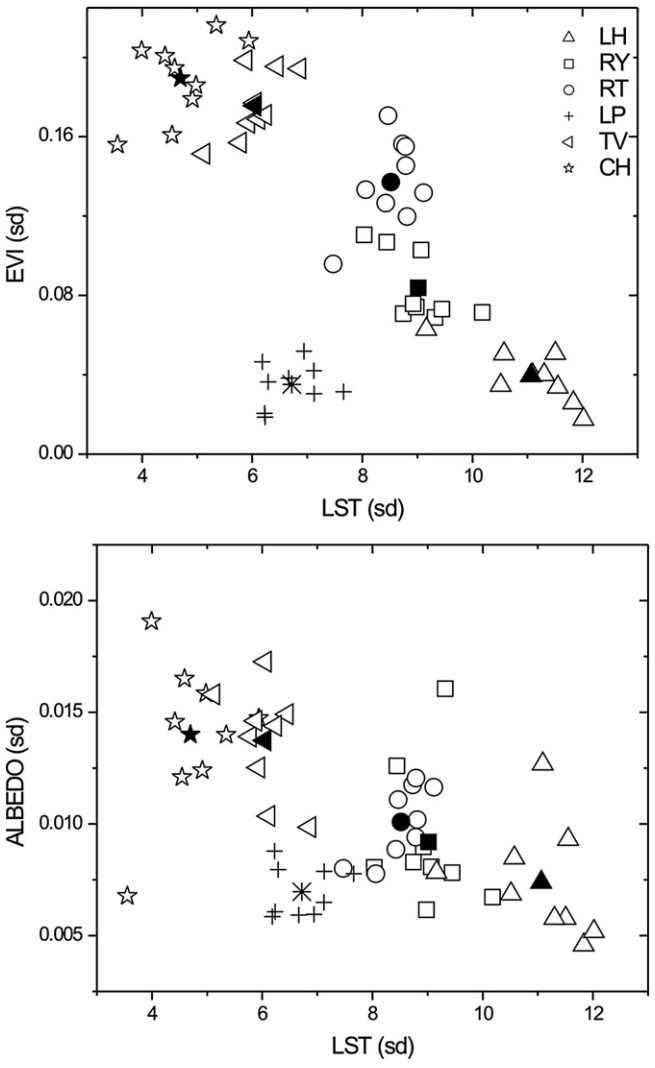

Fig. 3. The EVI, albedo and LST annual variabilities (standard deviations).

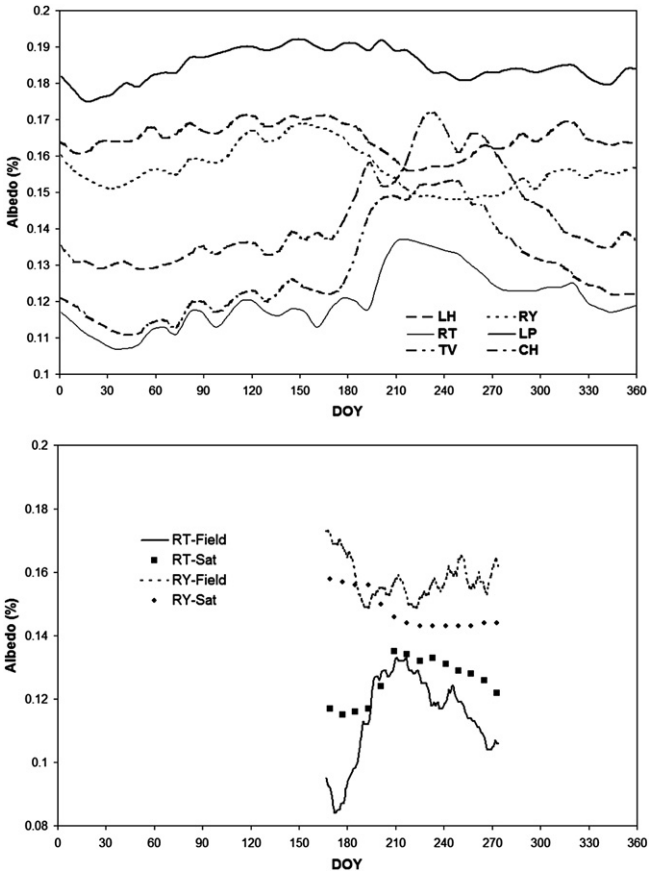

Fig. 4. The top plot, shows the albedo average seasonal variation within a year obtained from MODIS. The bottom plot shows a comparison between the average MODIS albedo value and average albedo from field observations measured with a radiometer for *RY* and *RT*.

3. Results and discussion

MODIS land cover classification process should be used with caution, since there are considerable sources of error that can result in a misclassification (Friedl, 2002). In any case, we can only say that there is a high probability that a specific class is of a certain type, due to all the averaging or smoothing methods used to estimate downscale prior probabilities at finer resolutions. The probabilities of being correct are high for dense vegetation covers (lcc 1–3), and sparse or barren (lcc 11–17). The vegetation land classes with intermediate vegetation cover are less certain (lcc 4–10). In our case, the MODIS land cover classification is correct for *LH*, *RY* and *TV*. Considering the three tropical deciduous forest sites, it is striking (and rather alarming) that only the TV site has been correctly classified. Nonetheless, all three sites show similar seasonal behavior, as will be seen below.

In Fig. 2, the seasonal EVI variation is observed for each site. The time resolution is 16 days from MODIS data sets. The green-up begins after DOY ≈ 145 (May 25th), when the vegetation index starts to increase from its dormant value as the summer wet season starts at each latitude from southern to northern regions along the west coast of the Sierra Madre Occidental and reaches its maximum at full maturity on DOY ≈ 273, (Sep. 30th), when they cease to grow and enter their senescent regime as the summer wet season subsides at each site. The maximum values are obtained at different dates due to the different types of vegetation, combined with the characteristics of the NAM precipitation regime, so that northern latitudes in the NAM region have shorter summer wet seasons than southern ones. Tropical deciduous forests show the largest changes in EVI values Δ_{EVI}, going from a minimum pre-monsoon EVI_{min} value to a maximum EVI_{max} value within the fully developed monsoon season. These values, growth and time lapse are presented in Table 3b. The NAM related precipitation begins at Chamela about one month prior to that in southern Arizona.

Méndez-Barroso et al. (2009) carried out a detailed study of the seasonal changes in EVI in the río Sonora watershed, using the same MODIS composite data sets employed here, for the 3 year period 2004–2007. They used as a metric D_{EVI} defined as $D_{EVI} = 100^*(EVI_{max}\text{-}EVI_{min})/EVI_{min}$ and the spatial distribution of D_{EVI} is presented (their Figure 3). When their results are compared with those presented here, it is striking that large areas in the rio Sonora have D_{EVI} greater than 300%, whereas the maximum for our sites is 272% for Chamela (Table 3b). These differences are not surprising when we remember that the values of EVI shown here in Fig. 2 and Table 3a,b, have been averaged spatially (20–30 km^2) and temporally (10 years) in order to present a clear description of the *average seasonal changes* in this region. It should also be noted that the largest values for D_{EVI} are usually obtained for cover types with very low values for EVI_{min}, not necessarily those with the largest values for ΔEVI. Nevertheless, Méndez-Barroso et al. (2009) show that small scale spatial variability is also very important in land cover types that were not included in this study, such as riparian deciduous woodland, savanna grassland and Madrean evergreen Woodland.

In Fig. 3a, plots of EVI vs. LST seasonal variability (standard deviations) are presented for each year. The solid symbol represents the average annual value for each site. We can distinguish two separate groups. The desert shrub and subtropical shrub sites *LH*, *RY*, present a low seasonal variability in EVI and large variations in LST. In this case, mean values for *LH*, $\sigma_{EVI} = 0.04$, $\sigma_{LST} = 11.1$ K and RY $\sigma_{EVI} = 0.084$, $\sigma_{LST} = 9.0$ K. At the other extreme, the deciduous tropical forests sites (*TV*, *CH*), show large seasonal variability in EVI and relatively small LST variations. For *TV*, $\sigma_{EVI} = 0.18$, $\sigma_{LST} = 6.0$ K, and for *CH*, $\sigma_{EVI} = 0.19$, $\sigma_{LST} = 4.7$ K. The *LP* site presents both small annual variability in EVI and LST, $\sigma_{EVI} = 0.04$, $\sigma_{LST} = 6.7$ K, compared with the other sites.

We continue with the analysis of Fig. 3a, with the aid of precipitation data that is available for the *RY* site. The average precipitation at *RY* is 475 mm $year^{-1}$, with 310 mm (65%) occurring during the summer wet season. There are three years with above average EVI variability ($\sigma_{EVI} = 0.08$), corresponding to years 2006 ($\sigma_{EVI} = 0.11$), 2007 ($\sigma_{EVI} = 0.10$), and 2008 ($\sigma_{EVI} = 0.11$). In 2006 the summer rainfall was 385 mm (80% of total), 449 mm (89% of total) in 2007 and 485 mm (89% of total) in 2008. Summer precipitation is the main driver of EVI summer growth in the NAM core region, as is observed in Fig. 2.

Table 3a
Summary of albedo α, EVI and LST changes in the NAM region between pre-monsoon DOY = 145 (May 25th) and fully developed monsoon DOY = 225 (Aug 13th).

	DOY = 145		DOY = 225			Variation			
Site	α	EVI	LST	α	EVI	LST	Δ_α	Δ_{EVI}	Δ_{LST}
LH	0.17	0.12	46	0.16	0.21	36	−0.01	0.09	−10
RY	0.17	0.15	47	0.15	0.41	34	−0.02	0.26	−13
RT	0.12	0.15	49	0.14	0.53	31	0.02	0.38	−18
LP	0.19	0.15	46	0.19	0.17	44	0.00	0.02	−2
TV	0.13	0.21	41	0.15	0.68	27	0.02	0.47	−14
CH	0.14	0.18	40	0.17	0.64	30	0.03	0.46	−10

Table 3b
Summary of EVI growth during the monsoon and time lapse Δt between minimum and maximum EVI values. The percentage increase is calculated as Δ_{EVI}/EVI_{min}.

Site	EVI_{min}	DOY_{min}	EVI_{max}	DOY_{max}	Δ_{EVI}	% increase	Δt days
LH	0.12	177	0.21	241	0.09	75	64
RY	0.15	161	0.41	225	0.26	173	64
RT	0.15	145	0.53	225	0.38	253	80
LP	0.14	161	0.23	257	0.09	64	96
TV	0.21	145	0.68	225	0.47	224	80
CH	0.18	145	0.67	241	0.49	272	96

The surface properties of the sites within the NAM region follow similar trends from northern to southern latitudes. Going from north to south, the LST variability decreases while the EVI and Albedo variability increases. Both EVI and Albedo variability show similar behavior as functions of LST variability.

In Fig. 3b, a plot of Albedo vs. LST season variability (standard deviation values) is presented, with average values in solid black color, following the same site nomenclature as that of Fig. 3a. In the albedo case, as before, two separate groups can be distinguished: the deciduous tropical forests (*CH*, *TV*), show a greater albedo seasonal variability and lesser LST variability. In *CH* case, $\sigma_{albedo} = 0.14$, $\sigma_{LST} = 4.7$ K, and in *TV* case, $\sigma_{albedo} = 0.14$, $\sigma_{LST} = 6.0$ K. In the case of *RT*, it is found that $\sigma_{albedo} = 0.10$, $\sigma_{LST} = 8.5$ K, which are now closer to *RY* values, $\sigma_{albedo} = 0.09$, $\sigma_{LST} = 9.0$ K. For *LH*, the average variability is $\sigma_{albedo} = 0.07$, $\sigma_{LST} = 11.1$ K. The subtropical and desert shrub vegetation regions have low albedo variability and large land surface temperature variability. All the previous five sites average variability, also fall along a line with negative slope, as in the case of EVI vs. LST, with the exception of *LP* site, for which $\sigma_{albedo} = 0.07$, $\sigma_{LST} = 6.7$ K.

The annual standard deviation (sd) in albedo, EVI and LST are seasonal summer/winter differences, so that there is a clear gradient with of sd for albedo and EVI increasing from north to south, while sd for LST decreases from north to south. The yearly sd values are displayed in Fig. 3 with 10 year averages in solid black. Méndez-Barroso and Vivoni (2010), do a similar study of NDVI, albedo and LST variability for the Río Sonora basin for a 3 year period (2004–2007).

In Fig. 4, the actual shortwave albedo from MODIS product MCD43A was averaged over years 2000–2008 to observe the seasonal albedo variations for each site, where small seasonal variations can be appreciated. We will consider DOY = 145 (May 25th), as the beginning of the monsoon season (green-up onset), and DOY = 273 (Sep. 30th) as the end of the monsoon season (senescence onset), and compute the changes in albedo $\Delta\alpha$ as the monsoon develops. These values are summarized in Table 3a.

From Table 3b data, we can distinguish two distinct vegetation classes. For *LH* and *RY*, which correspond to desert shrub and subtropical shrub, the albedo is high during the pre-monsoon season and decreases during the summer wet season. For *LH* the annual average albedo value is $\alpha_{ave} = 0.16$, attaining a minimum value of $\alpha_{min} = 0.16$ (DOY 217, Aug. 5th). Similarly, for *RY*, $\alpha_{ave} = 0.16$, with $\alpha_{min} = 0.15$ (DOY 257, Sep. 14th). For the three tropical deciduous forests sites, *RT*, *CH* and *TV*, the seasonal albedo variation shows the opposite behavior: the albedo increases as the vegetation develops in response to the summer rains. This result is rather surprising and will be analyzed in more detail below. So, for *RT*

$\alpha_{ave} = 0.12$ and $\alpha_{max} = 0.14$ (DOY 217, Aug. 5th), for *TV* $\alpha_{ave} = 0.13$ and $\alpha_{max} = 0.15$ (DOY 241, Aug. 29th) and for *CH* $\alpha_{ave} = 0.14$ *a*nd $\alpha_{max} = 0.17$ (DOY 233, Aug. 21th). The *LP* site has the highest albedo values in the region, *b*ut does not follow the same patterns as the rest of the sites during the NAM rainfall season, its albedo values *a*re $\alpha_{ave} = 0.18$ and $\alpha_{min} = 0.18$ (DOY 017, Jan. 17th), $\alpha_{max} = 0.19$ (DOY 145, May 25th). Both albedo extreme values for *LP* occur before the NAM summer wet season. These differences between summer and winter albedo for desert and subtropical shrub and tropical deciduous forests are due to differences in horizontal heterogeneity, leaf orientation, stomatal and leaf area, and total biomass. Albedo values for open and sparse vegetation regions are generally higher than those for tropical deciduous forests, as was found in similar work by Davidson and Wang (2005).

These variations are in agreement with similar results for seasonal albedo variations found for the northern hemisphere in the broad 20°N–50°N latitudinal band for black-sky albedo MODIS product MOD43B3 by Zhou, et al. (Fig. 3 Zhou et al., 2003). The higher (lower) values of albedo during winter and summer months for each class of land vegetation is also influenced by the latitude (Figs. 2a,b, Zhou et al., 2003). In Fig. 4, during winter months in the desert shrubs *LH* has higher albedo than *RY* due to its higher northern latitude, while in tropical deciduous forests *CH* has a higher albedo than *TV* and *RT*. The *LP* site, however, does not follow this behavior.

The bottom part of Fig. 4 shows a comparison between the average albedo value of a single MODIS pixel of 500 m resolution and average albedo from field observations measured with a radiometer for *RY* and *RT*. The available albedo field data used were from DOY 167–273 (Jun. 16th to Sep. 30th) for 2004, 2006, 2007 and 2008. Some discrepancies between the albedo product from MODIS satellite observations and averaged albedo field measurements can be observed. In the *RY* site case, the MODIS albedo products underestimate albedo values, compared to field observations, while in the *RT* site case, the opposite occurs. The field observations in *RY* (*RT*) are made with a radiometer located at ~7 m (~11 m) above the land surface and half the signal covers a 45° conic solid angle, which amounts to a sensible surface area of ~154 m^2 (~380 m^2), which includes a vegetation with top cover in the vicinity of ~4–5 m (~9–10 m). The observed satellite data for this comparison covered a single 500 m pixel, i.e. 250,000 m^2.

In the case of *RY* which is subtropical shrubs, MODIS underestimates the surface albedo, since the albedo computation algorithm depends on the land surface structure and optical properties for soil and fractional vegetation cover. The fractional vegetation cover and soil geometric properties are assumed by MODIS to be homogeneous for the whole 500 m pixel, while the radiometer measurements are representative of only a tiny fraction. So the discrepancies in the physical properties seen by the satellite and the radiometer near the land surface are hardly surprising. In the case of the tropical deciduous forest site *RT*, the MODIS albedo is larger than the field measurements. This may be due to the fact that satellites observe more sunlit gaps than would field measurements made near the top of the canopy (Zhou et al., 2003).

Nonetheless, in both cases, MODIS observed data and field observations show the same qualitative behavior, the albedo values decreasing for subtropical shrub and increasing for tropical deciduous forests during the summer wet season. The results in *RY* are consistent with the report by Méndez-Barroso and Vivoni (2010).

From Fig. 4, we can observe that there are clear differences between the behavior in the open shrubland sites (LH and RY) where albedo *decreases* after monsoon onset and the forest sites (RT, TV and CH) where the albedo *increases* after monsoon onset. Therefore, these five sites were divided into two groups according to the above and average values were calculated over all members for each time period. The results are shown in Fig. 5 with the average albedo of each group, as well as the difference between the two. It can be seen very clearly that the albedo for the shrubland (0.16) is about 0.04 higher than that for the forests (0.12) from January until the monsoon begins around the end of June. Afterwards, the difference between them decreases rapidly, being small (~0.01 or less) during the entire rainy season (July–September) when the foliage cover is maximum. After this, the difference increases slowly to return to its maximum value of around 0.04 in early January.

These results strongly suggest that soil reflectance is the major factor in determining the differences in albedo between the two cover types. The soils at the forest sites are darker than those for the shrubland sites, mainly due to increased organic content, although volcanic origin may also be a factor. Thus albedo of the shrublands is higher when vegetation cover is relatively low and the soil contributes significantly to the total surface reflectance. As the vegetation cover increases, this contribution decreases and becomes very small at full cover.

In Table 3a,b, a summary of surface characteristics is presented. The values of each of the averaged MODIS available data used in this study are presented for each of the six sites. A pre-monsoon stage (DOY 145, May 25th), that coincides with the date in which the EVI values attain a minimum (within the 16-day MODIS EVI products resolution) will be used as a reference to measure albedo, EVI and LST variations as the monsoon season begins. The fully developed monsoon stage is taken to be DOY 225 (Aug. 13th), where almost all sites have reached their maximum EVI seasonal value. The variations in albedo, EVI and LST are then presented.

Regarding albedo, EVI and mean LST, *LP* response during the monsoon season compared to others, does not reflect any significant change in an 80 days time period. Although this site is geographically close to the others, its surface characteristics respond to a completely different climate pattern, and so will be excluded in the following discussion of results of Table 3a,b.

The albedo values are of the same order for all sites in the pre-monsoon season, being slightly larger in northern desert shrub regions and smaller in southern tropical deciduous forests. It should be noted that, in open and sparse vegetation regions (*LH*, *RY*), the mean albedo values due to highly reflective surfaces *decrease* by the appearance of small amounts of organic matter, while in the higher dense vegetation regions as in tropical deciduous forests (*RT*, *TV*, *CH*) the mean albedo values *increase* due to greenness increase. All regions achieve similar albedo values during the fully developed monsoon, with values ranging between 0.13

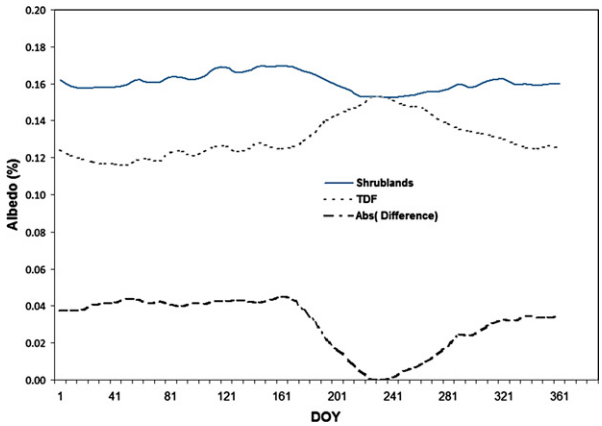

Fig. 5. Plot of average albedos of grouped vegetation, shrublands and tropical deciduous forests and albedo difference between the two groups.

Table 4
Summary of average daily values for surface measured quantities. P is precipitation (mm day^{-1}), Rn is the net incoming radiation (mm day^{-1}), ET refers to the Evapotranspiration (mm day^{-1}).

Variable	RY					RT				
	2004	2006	2007	2008	Average	2004	2006	2007	2008	Average
P	2.25	3.51	4.16	4.40	3.58	4.80	3.80	4.62	6.63	4.96
R_n	5.30	6.47	5.48	5.35	5.65	5.05	6.22	6.06	6.18	5.88
ET	1.90	3.02	3.55	3.50	2.99	3.25	2.99	3.20	4.16	3.40
ET/P	0.84	0.86	0.85	0.79	0.84	0.68	0.79	0.69	0.63	0.70
ET/R_n	0.36	0.47	0.65	0.65	0.53	0.64	0.48	0.53	0.67	0.58

and 0.16, Watts et al. (2007). On the other hand, EVI variations are largest in closed and dense vegetations, such as tropical deciduous forests and smallest in open and sparse vegetation, such as subtropical and desert shrub regions. As soon as the monsoon season starts, the average daytime LST drops by more than 10 °C, in response to the increase in vegetation cover and soil moisture produced by the rains. It is interesting to note that the largest decrease in LST occurs at the central site *RT* (−18 °C) and the magnitude of the change is progressively smaller for sites further north or further south. Indeed, there is a pleasing symmetry in these observations, although this is presumably fortuitous. In Table 4, a summary of the average surface conditions are presented for both *RY* and *RT* sites. In *RY* there is less average precipitation 3.6 mm day^{-1} compared to that in *RT* of 5.0 mm day^{-1}. The net radiation R_n, is about the same in both sites due to their proximity, a 4% difference larger in *RT* than *RY*. While the average ET measured in *RY* (3.0 mm day^{-1}) is less than that in *RT* (3.4 mm day^{-1}), the ratio of evapotranspiration to precipitation is greater in *RY* (ET/P = 0.84) compared to that in *RT* (ET/P = 0.70), reflecting more efficient water use by the *RY* vegetation system than that for *RT*. In general, vegetation in arid sites are adapted to use the scarce supply of water much more efficiently than tropical vegetation, where there is a surplus of available water. Finally, the evaporative fraction, the fraction of available net radiation used in evapotranspiration, is slightly lower in *RY* (ET/R_n = 0.53) than in *RT* (ET/R_n = 0.58). All these results are consistent with previous results (Watts, et al., 2007) that were obtained using data for the 2004 Monsoon season only.

4. Conclusions

The MODIS land cover classification was correct for all the open shrub sites (*LH*, *RY*, *LP*) but only one of the three deciduous forest sites (*TV*). The others were misclassified, *RT* as Barren and *CH* as Cropland. Nonetheless, all three sites show similar behavior: *TV* and *CH* are almost identical while *RT* clearly belongs to the same family. This land cover classification may not have resulted with good accuracy for some of the vegetation types in our studied sites, i.e., that each specific pixel selected has a determined probability of belonging to a specific land cover class in that specific geographical location, still each site is dominated by a strong vegetation type signal as described in Table 1 (*LH*, *LP* and *RY* being desert shrubs and subtropical shrub, and *RT*, *TV*, *CH* being tropical deciduous forests).

Very large variations were observed in the seasonal EVI index triggered by the onset of the summer wet season, but the albedo variation is less marked. The albedo in subtropical shrub and desert shrub regions decreases (6–12% less) while there is a large increase in EVI (75–175% more). In the specific case of *LP*, there a small increase in EVI (13%), but no significant change in albedo in the same time period. In contrast, in the tropical deciduous forests, both albedo and EVI increase during the warm summer wet season (16-21% larger albedo and 220–255% increase in EVI). This increase in albedo for the tropical vegetation was reported previously for the *RT* site (Watts et al., 2007) and is now seen to be characteristic of the tropical deciduous forest. It appears that this behavior is mainly due to differences in soil albedo, which makes a significant contribution to total surface albedo in the dry, pre-monsoon conditions, but becomes less important as the vegetation cover increases in response to the monsoon rains. Thus for maximum cover (around mid August) the observed albedo is very similar at all sites. A more detailed study over a wide area will be necessary to confirm (or refute) this suggestion.

All sites show a general average decrease in LST from the pre-monsoon values as the monsoon season fully develops, being moderate (∼10 °C) in upper northern (*LH*) and lower southern regions (*CH*) and larger (∼14 °C) at mid latitudes (*RY*, *TV*), with a maximum LST drop (∼18 °C) in *RT*. Again, *LP* only shows a very small (∼2 °C) mean decrease in LST. Thus we can conclude that the surface characteristics at the LP site show a completely different behavior to the other sites considered in this study. LP may be geographically close to other sites, but its climatology is completely different and does not show any influence from the NAM system.These sharp decreases in LST will reduce the outgoing longwave radiation and so tend to increase net radiation at the surface, assuming that the solar radiation remains roughly constant. However, it is likely that there will be an increase in cloudiness after the monsoon onset, which will tend to reduce incoming solar radiation, so that the change in net radiation may be quite small in many cases (Méndez-Barroso and Vivoni, 2010).

The EVI summer growth in the NAM region relies on the timing and intensity of the precipitation. If the rains are delayed or the precipitation occurs as occasional, high intensity events, then optimum vegetation development (EVI growth) may not be attained, since the excess water will run off after the soil reaches saturation, so that it does not contribute to plant growth. In general, there will be increased vegetation growth when the precipitation is above average but spatial variability will also be very high (Méndez-Barroso et al., 2009; Méndez-Barroso and Vivoni, 2010).

It should be mentioned that this study has some limitations. For example, the satellite products only select cloud free conditions so the expected increase in cloudiness after monsoon onset is not addressed here. Also, only 6 sites have been selected for analysis. Surface fluxes of radiation, heat, water vapor and CO_2 are measured at the three northern sites (LH, RY and TP) and similar measurements at the southern sites would allow more detailed analyses to be undertaken, linking these fluxes to the satellite observations over the entire region.

Acknowledgements

The authors wish to thank all the agencies that have directly supported this research and without their financial support it would be impossible to obtain these results: CONACYT, NOAA. Also we would like to thank Dave Gochis from UCAR, Michael Douglas from NOAA, Enrique Vivoni from Arizona State University for their fruitful discussions and comments.

References

Davidson, A., Wang, S., 2005. Spatiotemporal variations in land surface albedo across Canada from MODIS observations. Can. J. Remote. Sens. 31 (5), 377–390.
Douglas, M.W., Maddox, R.A., Howard, K., Reyes, S., 1993. The mexican monsoon. J. Climate 6, 1665–1677.
European Commission, DG AGRI, EUROSTAT and the Joint Research Centre (Ispra), European Environment Agency, 2000. From Land Cover to Landscape Diversity in the European Union. http://ec.europa.eu/agriculture/publi/landscape/index.htm Available online at:Last visited December 27th, 2008.
Friedl, M., 2002. Validation of the Consistent-year V003 MODIS Land Cover Product. Available online at: http://landval.gsfc.nasa.gov/pdf/MOD12_supporting_materials.PDF Last visited on February 20th, 2009.

García-Oliva, F., Maass, J.M., Galicia, L., 1995. Rainstorm analysis and rainfall erosivity of a seasonal tropical region with a strong cyclonic influence on the pacific coast of Mexico. J. Appl. Meteor. 34, 2491–2498.

Gochis, D.J., Leal, J.C., Shuttleworth, W.J., Watts, C.J., Garatuza-Payan, J., 2003. Preliminary diagnostics from a new event-based precipitation monitoring system in support of the North American Monsoon Experiment. J. Hydrometeor. 4, 974–981.

Gochis, D.J., Jimenez, A., Watts, C.J., Garatuza-Payán, J., Shuttleworth, W.J., 2004. Analysis of 2002 and 2003 warm-season precipitation from the North American monsoon experiment rain gauge network. Mon. Weather Rev. 132, 2938–2953.

Gochis, D.J., Brito-Castillo, L., 2006. Hydroclimatology of the North American Monsoon Region in North west Mexico. J. Hydrol. 316, 53–70.

Gochis, D.J., Watts, C.J., Garatuza-Payán, J., Rodriguez, J.C., 2007. Spatial and temporal patterns of precipitation intensity as observed by the NAME Event Rain Gauge Network from 2002 to 2004. J. Climate 20, 1734–1750.

Higgins, R.W., Yao, Y., Wang, X.L., 1997. Influence of the North American Monsoon system on the U.S. summer precipitation regime. J. Climate 10, 2600–2622.

Higgins, W., Gochis, D.J., 2007. A Synthesis of the results from the North American Monsoon Experiment (NAME). J. Climate 20, 1601–1607.

Huete, A., Justice, C., van Leeuwen, W., 1999. MODIS Vegetation index, Algorithm Theoretical Basis Document, Version 3. Available online at: http://modis.gsfc.nasa.gov/data/atbd/atbd_mod13.pdf Last visited December 26th, 2008.

Huete, A., Didan, K., Miura, T., Rodriguez, E.P., Gao, X., Ferreira, L.G., 2002. Overview of the radiometric and biophysical performance of the MODIS vegetation indexes. Remote Sens. Environ. 83, 195–213.

Iqbal, M., 1984. Introduction to Solar Radiation. Academic Press Inc.

Maass, J.M., Vose, J.M., Swank, W.T., Martinez-Yrizar, A., 1995. Seasonal changes of leaf area index (LAI) in a tropical deciduous forest in west Mexico. For. Ecol. Manage. 74, 171–180.

Méndez-Barroso, L.A., Vivoni, E.R., 2010. Observed shifts in land surface conditions during the North American Monsoon: implications for a vegetation-rainfall feedback mechanism. J. Arid Environ. 74, 549–555.

Méndez-Barroso, L.A., Vivoni, E.R., Watts, C.J., Rodríguez, J.C., 2009. Seasonal and interannual relation between precipitation, surface soil moisture and vegetation dynamics in the North American monsoon regional. J. Hydrol. 377, 59–70.

CPC-NWS, 2008. US-Mexico Climatology (Annual Cycle). Available online:. Climate Prediction Center, National Weather Service http://www.cpc.noaa.gov/products/precip/CWlink/clim.table.html Last visited on December 29th, 2008.

Salinas-Zavala, C.A., Douglas, A.V., Diaz, H.F., 2001. Interannual variability of NDVI in northwest México. Associated Climatic Mechanism and Ecological Implications. Remote Sens. Environ. 82, 417–430.

Schaaf, C.B., Gao, F., Strahler, A.H., Lucht, W., Li, X., Tsang, T., Strugnell, N.C., Zhang, X., Jin, Y., Muller, J.-P., Lewis, P., Barnsley, M., Hobson, P., Disney, M., Roberts, G., Dunderdale, M., Doll, C., d'Entremont, R., Hu, B., Liang, S., Privette, J.L., 2002. First operational BRDF, Albedo and Nadir reflectance products from MODIS. Remote Sens. Environ. 83, 135–148.

Strahler, A.H., Lucht, W., Schaaf, C.B., Tsang, T., Gao, F., Li, X., Muller, J.-P., Lewis, P., Barnsley, M.J., 1999a. MODIS BRDF/Albedo Product, Algorithm Theoretical Basis Document. Available online at: http://modis.gsfc.nasa.gov/data/atbd/atbd_mod09.pdf Last visited on December 26th, 2008.

Strahler, A.H., Muchoney, D., Borak, J., Friedl, M., Gopal, S., Lambin, E., Moody, A., 1999b. MODIS Land Cover Product, Algorithm Theoretical Basis Document. Available online at: http://modis.gsfc.nasa.gov/data/atbd/atbd_mod12.pdf Last visited on February 20th, 2009.

Vivoni, E.R., Rodriguez, J.C., Watts, C.J., in press. On the spatiotemporal variability of soil moisture and evapotranspiration in a mountainous basin within the North American Monsoon Region, Water Resources Research.

Vivoni, E.R., Moreno, H.A., Mascaro, G., Rodríguez, J.C., Watts, C.J., Garatuza-Payan, J., Scott, R.L., 2008. Observed relation between evapotranspiration and soil moisture in the North American monsoon region. Geophys. Res. Lett. 35, L22403. doi:10.1029/2008GL036001.

Wan, Z., 1999. MODIS Land-Surface Temperature, Algorithm Theoretical Basis Document, Version 3.3. Available online at: http://modis.gsfc.nasa.gov/data/atbd/atbd_mod11.pdf Last visited December 26th, 2008.

Watts, C.J., Scott, R.L., Garatuza-Payán, J., Rodriguez, J.C., Prueger, J.H., Kustas, W.P., Douglas, M.D., 2007. Changes in vegetation condition and surface fluxes during NAME 2004. J. Climate 20, 1810–1820.

Zhang, X., Friedl, M.A., Schaaf, C.B., Strahler, A.H., Hodges, J.C.F., Gao, F., Reed, B.C., Huete, A., 2003. Monitoring vegetation phenology using MODIS. Remote Sens. Environ. 84, 471–475.

Zhou, L., Dickinson, R.E., Tian, Y., Zeng, X., Dai, Y., Yang, Z.-L., Schaaf, C.B., Gao, F., Jin, Y., Strahler, A., Myneni, R.B., Yu, H., Wu, W., Shaikh, M., 2003. Comparison of seasonal and spatial variations of albedos from Moderate-Resolution Imaging Spectroradiometer (MODIS) and Common Land Model. J. Geophys. Res. 108 (D15), 4488. doi:10.1029/2002JD003326.